Journal of Solid Mechanics Vol. 10, No. 4 (2018) pp. 804-815

Delamination of Two-Dimensional Functionally Graded Multilayered Non-Linear Elastic Beam - an Analytical Approach

V. Rizov *

Department of Technical Mechanics, University of Architecture, Civil Engineering and Geodesy, Bulgaria

Received 21 July 2018; accepted 23 September 2018

ABSTRACT

Delamination fracture of a two-dimensional functionally graded multilayered four-point bending beam that exhibits non-linear behaviour of the material is analyzed. The fracture is studied analytically in terms of the strain energy release rate. The beam under consideration has an arbitrary number of layers. Each layer has individual thickness and material properties. A delamination crack is located arbitrary between layers. The material is two-dimensional functionally graded in the cross-section of each layer. The beam mechanical behaviour is described by a power-law stress-strain relation. The fracture is analyzed also by applying the *J*-integral approach in order to verify the solution derived for the strain energy release rate. The effects of crack location, material gradient and non-linear behaviour of material on the delamination fracture are evaluated. It is found that the material non-linearity leads to increase of the strain energy release rate. Therefore, the material non-linearity should be taken into account in fracture mechanics based safety design of two-dimensional functionally graded multilayered structural members. It is found also that the delamination behaviour can be effectively regulated by using appropriate material gradients in the design stage of functionally graded multilayered structural members and components.

Keywords: Two-dimensional functionally graded material; Multilayered structure; Delamination; Material non-linearity; Analytical approach.

1 INTRODUCTION

NOWADAYS, functionally graded materials have been widely applied in various branches of modern industry such as aeronautics, electronics, engineering, optics and biomedicine [1-8]. These novel materials are made from a mixture of two or more different materials with continuous variation of properties in certain directions. Therefore, functionally graded materials are very suitable for structural members and components subjected to non-uniform service requirements. Since no distinct internal boundaries exist, failures from interfacial stress concentrations in functionally graded materials are largely avoided in contrast to conventional fiber reinforced composites [9, 10]. The performance of structural members made of functionally graded materials depends strongly

* Corresponding author. Tel.: + 359-2 963 52 45 / 664; Fax: + 359-2 86 56 863.
E-mail address: V_RIZOV_FHE@UACG.BG (V.Rizov).

on their fracture behaviour [11-16]. Studies of fracture behaviour of functionally graded materials have been reviewed in [12]. Solutions of various crack problems by using methods of linear-elastic fracture mechanics have been considered. Analyses of cracks oriented both parallel and perpendicular to the material gradient direction have been summarized. Fracture behaviour under static and fatigue crack loading conditions has been investigated. Works on rectilinear cracks, circular arc cracks and slightly curved cracks in functionally graded structural members have been presented. Cracks and re-entrant corners in functionally graded components have been analyzed assuming linear-elastic behaviour of the material [13]. A method for evaluating the strength of structures composed by functionally graded materials has been developed. For this purpose, linear-elastic fracture mechanics has been applied. The validity of the method has been shown by investigating the fracture behaviour of rectangular plates in tension and beams under three-point bending containing re-entrant corners. Different corner angle and depth have been considered. Analyses of cracked three-point bending beams made of functionally graded material have been developed in [14]. The compliance approach for evaluation of fracture behaviour has been explored. An equivalent homogeneous beam of variable height for cracked functionally graded beams has been suggested. Linear-elastic behaviour of the functionally graded material has been assumed. The rate of change of the compliance has been evaluated. It has been found that the equivalent homogeneous beam with cubic variation of the height is the most suitable for capturing the compliance characteristics of the functionally graded beam under consideration. The analysis has shown that the method developed can also be applied for other cracked functionally graded linear-elastic components under concentrated loads. Multilayered materials are inhomogeneous materials manufactured by bonding many single layers of different properties [17, 18]. The design ability of multilayered materials makes them a promising alternative to commonly used metals. However, multilayered materials are highly susceptible to delamination fracture. Therefore, accessing of structural integrity and safety of multilayered materials necessities profound knowledge of their delamination behaviour [19, 20].

The present paper is focused on delamination fracture behaviour of two-dimensional functionally graded multilayered four-point bending beam configuration exhibiting material non-linearity. The delamination is studied analytically in terms of the strain energy release rate. The non-linear mechanical behaviour is described by using a power-law stress-strain relation. The influence of crack location, material gradient and material non-linearity on the fracture is investigated.

2 ANALYSIS OF THE STRAIN ENERGY RELEASE RATE

The present paper deals with delamination fracture analysis of the functionally graded multilayered four-point bending beam configuration shown in Fig. 1. The beam is made of an arbitrary number of horizontal layers. Perfect adhesion is assumed between layers. Each layer has individual thickness and material properties. A vertical notch of dept, h_2, is cut the beam mid-span in order to generate conditions for delamination fracture. A delamination crack of length, $2a$, is located symmetrically with respect to the beam mid-span. The lower and upper crack arm thicknesses are denoted by h_1 and h_2, respectively. The beam is loaded in four-point bending by two vertical forces, F, applied at the beam free ends. It should be noted that the delamination crack is located in the beam portion between the two supports (this beam portion is loaded in pure bending). It is obvious, that the upper crack arm is free of stresses (Fig. 1). The beam non-linear mechanical behaviour is described by power-law stress-strain relation [21]

$$\sigma_i = S_i \varepsilon^{n_{fi}} \quad , \; i = 1, 2, ..., n \tag{1}$$

where σ_i is the distribution of normal stresses in the i-th layer, S_i and n_{fi} are material properties in the same layer, n is the number of layers, ε is the longitudinal strains distribution. The material in each layer is two-dimensional functionally graded. The material property, S_i, varies continuously in the i-th layer cross-section according to the following law:

$$S_i = S_{Ui} + \frac{S_{Li} - S_{Ui}}{z_{1i+1} - z_{1i}} \left(z_1 - z_{1i} \right) + \frac{16 S_{Ai}}{b^4} y_1^4 \tag{2}$$

where

$$-\frac{b}{2} \le y_1 \le \frac{b}{2} \ , \ z_{1i} \le z_1 \le z_{1i+1} \ , \ i = 1, 2, ..., n \tag{3}$$

In Eq. (2), S_{Ui} and S_{Li} are, respectively, values of S_i in the upper and lower surfaces of the *i*-th layer, S_{Ai} is a material property that governs the material gradient along the beam width, z_{1i} and z_{1i+1} are the coordinates of the upper and lower surfaces of the *i*-th layer, respectively (Fig. 2). Eq. (2) indicates that S_i is distributed symmetrically with respect to z_1 -axis.

It should be specified that the present analysis is valid for non-linear elastic behaviour of material. The analysis is applicable also for elastic-plastic behaviour if the beam undergoes active deformation, i.e. if the external loading increases only [22]. Besides, the present analysis is based on the small strain assumption.

In order to derive the strain energy release rate, *G*, an increase, Δa, of the crack length is assumed (the external load is kept constant). Thus, *G* is written as:

$$G = \frac{\Delta W_{ext} - \Delta U}{\Delta A} \tag{4}$$

where the change of external work is

$$\Delta W_{ext} = \Delta U + \Delta U^* \tag{5}$$

In Eq. (5), ΔU and ΔU^* are the changes of strain energy and complementary strain energy, respectively. The increase of crack area is

$$\Delta A = b \Delta a \tag{6}$$

By combining of Eqs. (4), (5) and (6), one obtains

$$G = \frac{\Delta U^*}{b \Delta a} \tag{7}$$

where the change of complementary strain energy is

$$\Delta U^* = U_a^* - U_b^* \tag{8}$$

In Eq. (7), U_a^* and U_b^* are the complementary strain energies after and before the increase of crack, respectively. From Eqs. (6) and (7), one obtains

$$G = \frac{U_a^* - U_b^*}{b \Delta a} \tag{9}$$

where

$$U_a^* = U_{aL}^* + U_{aU}^* \tag{10}$$

In Eq. (10), U_{aL}^* and U_{aU}^* are, respectively, the complementary strain energies in the lower and upper crack arm after the increase of crack length. Obviously, $U_{aU}^* = 0$ since the upper crack arm is free of stresses (Fig. 1). It should be noted that due to the symmetry, only the right-hand half of the beam is considered in the analysis.

The quantity, U_{aL}^*, is derived by integrating the complementary strain energy density in a portion of the lower crack arm of length, Δa, behind the crack tip

$$U_{aL}^{*}=\Delta a\sum_{i=1}^{i=n_L}\int_{z_{1i}}^{z_{1i+1}}\left(\int_{-\frac{b}{2}}^{\frac{b}{2}}u_{0i}^{*}dy_1\right)dz_1 \tag{11}$$

where n_L is the number of layers in the lower crack arm, u_{0i}^{*} is the complementary strain energy density in the *i*-th layer. The quantity, u_{0i}^{*}, is equal to the area, *OQR*, that supplements the area, *OPQ*, enclosed by the stress-strain curve to a rectangle (Fig. 3). Thus, u_{0i}^{*} is written as:

$$u_{0i}^{*}=\sigma\varepsilon-\int_{0}^{\varepsilon}\sigma d\,\varepsilon \tag{12}$$

The distribution of ε is analyzed by applying the Bernoulli' hypothesis for plane sections since the span to height ratio of the beam under consideration is large. Concerning the distribution of ε in the beam portion between the two supports, it should be noted that since this beam portion is loaded in pure bending, ε is the only non-zero strain. Thus, according to the small strain compatibility equation, ε is distributed linearly along the lower crack arm cross-section height

$$\varepsilon=\kappa_L\left(z_1-z_{1n_1}\right) \tag{13}$$

where κ_L is the curvature of lower crack arm, z_{1n_1} is the neutral axis coordinate (Fig. 2). It should be noted that the neutral axis, n_1-n_1, shifts from the centroid, since the beam is functionally graded and multilayered. The quantities, κ_L and z_{1n_1}, are determined from the following equations for equilibrium of the lower crack arm cross-section:

$$N=\sum_{i=1}^{i=n_L}\int_{z_{1i}}^{z_{1i+1}}\left(\int_{-\frac{b}{2}}^{\frac{b}{2}}\sigma_i dy_1\right)dz_1 \tag{14}$$

$$M=\sum_{i=1}^{i=n_L}\int_{z_{1i}}^{z_{1i+1}}\left(\int_{-\frac{b}{2}}^{\frac{b}{2}}\sigma_i z_1 dy_1\right)dz_1 \tag{15}$$

where *N* and *M* are, respectively, the axial force and the bending moment in the lower crack arm. It is obvious that (Fig. 1)

$$N=0\ ,\ M=Fl \tag{16}$$

The following equations are derived after substituting of Eqs. (1), (2) and (13) in Eqs. (14) and (15):

$$\begin{aligned}N=b\sum_{i=1}^{i=n_L}\kappa_L^{n_{fi}}\Bigg\{&\frac{S_{A_i}}{5\left(n_{fi}+1\right)}\left[\left(z_{1i+1}-z_{1n_1}\right)^{n_{fi}+1}-\left(z_{1i}-z_{1n_1}\right)^{n_{fi}+1}\right]+\\&+\frac{1}{n_{fi}+1}\left[\frac{1}{2}\left(S_{Ui}+S_{Li}\right)+\frac{1}{z_{1i+1}-z_{1i}}\left(S_{Li}-S_{Ui}\right)z_{1n_1}\right]\left[\left(z_{1i+1}-z_{1n_1}\right)^{n_{fi}+1}-\left(z_{1i}-z_{1n_1}\right)^{n_{fi}+1}\right]+\\&+\frac{1}{z_{1i+1}-z_{1i}}\left(S_{Li}-S_{Ui}\right)\frac{1}{n_{fi}+2}\left[\left(z_{1i+1}-z_{1n_1}\right)^{n_{fi}+2}-\left(z_{1i}-z_{1n_1}\right)^{n_{fi}+2}\right]\Bigg\}\end{aligned} \tag{17}$$

$$
\begin{aligned}
M = b\sum_{i=1}^{i=n_L} \kappa_L^{n_{fi}} \Bigg\{ & \frac{S_{A_i}}{5(n_{fi}+2)}\Big[\left(z_{1i+1}-z_{1n_1}\right)^{n_{fi}+2}-\left(z_{1i}-z_{1n_1}\right)^{n_{fi}+2}\Big]+ \\
& +\frac{S_{A_i} z_{1n_1}}{5(n_{fi}+1)}\Big[\left(z_{1i+1}-z_{1n_1}\right)^{n_{fi}+1}-\left(z_{1i}-z_{1n_1}\right)^{n_{fi}+1}\Big]+ S_{Ui}\Bigg\{ \frac{1}{n_{fi}+2}\Big[\left(z_{1i+1}-z_{1n_1}\right)^{n_{fi}+2}-\left(z_{1i}-z_{1n_1}\right)^{n_{fi}+2}\Big]+ \\
& +\frac{1}{n_{fi}+1}\Big[\left(z_{1i+1}-z_{1n_1}\right)^{n_{fi}+1} z_{1n_1}-\left(z_{1i}-z_{1n_1}\right)^{n_{fi}+1} z_{1n_1}\Big]\Bigg\}+ \\
& +\frac{1}{2}\left(S_{Li}-S_{Ui}\right)\Bigg\{ \frac{1}{n_{fi}+2}\Big[\left(z_{1i+1}-z_{1n_1}\right)^{n_{fi}+2}-\left(z_{1i}-z_{1n_1}\right)^{n_{fi}+2}\Big]+ \\
& +\frac{z_{1n_1}}{n_{fi}+1}\Big[\left(z_{1i+1}-z_{1n_1}\right)^{n_{fi}+1}-\left(z_{1i+1}-z_{1n_1}\right)^{n_{fi}+1}\Big]\Bigg\}+ \frac{1}{z_{1i+1}-z_{1i}}\left(S_{Li}-S_{Ui}\right)\Bigg\{ \frac{1}{n_{fi}+3}\Big[\left(z_{1i+1}-z_{1n_1}\right)^{n_{fi}+3}-\left(z_{1i}-z_{1n_1}\right)^{n_{fi}+3}\Big]+ \\
& +\frac{2z_{1n_1}}{n_{fi}+2}\Big[\left(z_{1i+1}-z_{1n_1}\right)^{n_{fi}+2}-\left(z_{1i}-z_{1n_1}\right)^{n_{fi}+2}\Big]+ +\frac{z_{1n_1}^2}{n_{fi}+1}\Big[\left(z_{1i+1}-z_{1n_1}\right)^{n_{fi}+1}-\left(z_{1i}-z_{1n_1}\right)^{n_{fi}+1}\Big]\Bigg\}\Bigg\}
\end{aligned}
\tag{18}
$$

Eqs. (17) and (18) should be solved with respect to κ_L and z_{1n_1} by using the Matlab computer program. It is obvious that at $n_{fi}=1$ the non-linear stress-strain relation (1) transforms into the Hooke's law. This means that $n_{fi}=1$ Eq. (18) should transform in the formula for curvature of linear-elastic beam. Indeed, by substituting of $n_{fi}=1$, $S_{Ui}=S_{Li}=E$ (E is the modulus of elasticity), $S_{Ai}=0$ and $n_L=1$ in Eq. (18), one obtains

$$
\kappa_L=\frac{12M}{Ebh_1^3} \tag{19}
$$

which is exact match of the formula for the curvature of linear-elastic homogeneous beam [23].

By substituting of Eqs. (1), (2) and (13) in Eq. (11), one derives

$$
\begin{aligned}
U_{aL}^{*} = b\Delta a\sum_{i=1}^{i=n_L}\Bigg\{ & \frac{\kappa_L^{n_{fi}+1} S_{Ai} n_{fi}}{5(n_{fi}+1)(n_{fi}+2)}\Big[\left(z_{1i}-z_{1n_1}\right)^{n_{fi}+2}-\left(z_{1i+1}-z_{1n_1}\right)^{n_{fi}+2}\Big]+ \\
& +\frac{\kappa_L^{n_{fi}+1} S_{Ui}}{(n_{fi}+1)(n_{fi}+2)}\Big[\left(z_{1i}-z_{1n_1}\right)^{n_{fi}+2}-\left(z_{1i+1}-z_{1n_1}\right)^{n_{fi}+2}\Big]+ \\
& +\frac{\kappa_L^{n_{fi}+1}\left(S_{Li}-S_{Ui}\right)}{n_{fi}+1}\Bigg\{ \frac{1}{2(n_{fi}+2)}\Big[\left(z_{1i}-z_{1n_1}\right)^{n_{fi}+2}-\left(z_{1i+1}-z_{1n_1}\right)^{n_{fi}+2}\Big]+ \\
& +\frac{1}{(z_{1i+1}-z_{1i})(n_{fi}+3)}\Big[\left(z_{1i}-z_{1n_1}\right)^{n_{fi}+3}-\left(z_{1i+1}-z_{1n_1}\right)^{n_{fi}+3}\Big]+ \\
& +\frac{z_{1n_1}}{(z_{1i+1}-z_{1i})(n_{fi}+2)}\Big[\left(z_{1i}-z_{1n_1}\right)^{n_{fi}+2}-\left(z_{1i+1}-z_{1n_1}\right)^{n_{fi}+2}\Big]\Bigg\}+ \kappa_L^{n_{fi}+1}\Bigg\{ \frac{S_{Ui}}{n_{fi}+2}\Big[\left(z_{1i+1}-z_{1n_1}\right)^{n_{fi}+2}-\left(z_{1i}-z_{1n_1}\right)^{n_{fi}+2}\Big]+ \\
& +\frac{S_{Li}-S_{Ui}}{2(n_{fi}+2)}\Big[\left(z_{1i+1}-z_{1n_1}\right)^{n_{fi}+2}-\left(z_{1i}-z_{1n_1}\right)^{n_{fi}+2}\Big]+\frac{S_{Li}-S_{Ui}}{(z_{1i+1}-z_{1i})(n_{fi}+3)}\Big[\left(z_{1i+1}-z_{1n_1}\right)^{n_{fi}+3}-\left(z_{1i}-z_{1n_1}\right)^{n_{fi}+3}\Big]+ \\
& +\frac{z_{1n_1}\left(S_{Li}-S_{Ui}\right)}{(z_{1i+1}-z_{1i})(n_{fi}+2)}\Big[\left(z_{1i+1}-z_{1n_1}\right)^{n_{fi}+2}-\left(z_{1i}-z_{1n_1}\right)^{n_{fi}+2}\Big]\Bigg\}\Bigg\}
\end{aligned}
\tag{20}
$$

where κ_L and z_{1n_1} are determined from Eqs. (17) and (18).

The complementary strain energy, U_b^*, before the increase of crack length is obtained by integrating the complementary strain energy density in a beam portion of length, Δa, ahead of the crack tip. Obviously, Eq. (20) can be applied also to calculate U_b^*. For this purpose, z_{1i}, z_{1i+1}, n_L, κ_L and z_{1n_1} should be replaced with z_{3i}, z_{3i+1}, n, κ and z_{3n_3}, respectively (κ and z_{3n_3} are the curvature and the coordinate of neutral axis of the cross-section of un-cracked beam portion ahead of the crack tip). The same replacements should be done in equilibrium Eqs. (17) and (18) in order to determine κ and z_{3n_3}.

The strain energy release rate is derived by doubling the expression obtained by substituting of U_a^* and U_b^* in Eq. (9) since there are two symmetric cracks (Fig. 1)

$$
\begin{aligned}
G = 2\sum_{i=1}^{i=n_L}\Bigg\{ & \frac{\kappa_L^{n_{fi}+1}S_{Ai}n_{fi}}{5(n_{fi}+1)(n_{fi}+2)}\left[\left(z_{1i}-z_{1n_1}\right)^{n_{fi}+2}-\left(z_{1i+1}-z_{1n_1}\right)^{n_{fi}+2}\right]+ \\
& +\frac{\kappa_L^{n_{fi}+1}S_{Ui}}{(n_{fi}+1)(n_{fi}+2)}\left[\left(z_{1i}-z_{1n_1}\right)^{n_{fi}+2}-\left(z_{1i+1}-z_{1n_1}\right)^{n_{fi}+2}\right]+ \\
& +\frac{\kappa_L^{n_{fi}+1}(S_{Li}-S_{Ui})}{n_{fi}+1}\Bigg\{ \frac{1}{2(n_{fi}+2)}\left[\left(z_{1i}-z_{1n_1}\right)^{n_{fi}+2}-\left(z_{1i+1}-z_{1n_1}\right)^{n_{fi}+2}\right]+ \\
& +\frac{1}{(z_{1i+1}-z_{1i})(n_{fi}+3)}\left[\left(z_{1i}-z_{1n_1}\right)^{n_{fi}+3}-\left(z_{1i+1}-z_{1n_1}\right)^{n_{fi}+3}\right]+\frac{z_{1n_1}}{(z_{1i+1}-z_{1i})(n_{fi}+2)}\left[\left(z_{1i}-z_{1n_1}\right)^{n_{fi}+2}-\left(z_{1i+1}-z_{1n_1}\right)^{n_{fi}+2}\right]\Bigg\}+ \\
& +\kappa_L^{\,n_{fi}+1}\Bigg\{ \frac{S_{Ui}}{n_{fi}+2}\left[\left(z_{1i+1}-z_{1n_1}\right)^{n_{fi}+2}-\left(z_{1i}-z_{1n_1}\right)^{n_{fi}+2}\right]+\frac{S_{Li}-S_{Ui}}{2(n_{fi}+2)}\left[\left(z_{1i+1}-z_{1n_1}\right)^{n_{fi}+2}-\left(z_{1i}-z_{1n_1}\right)^{n_{fi}+2}\right]+ \\
& +\frac{S_{Li}-S_{Ui}}{(z_{1i+1}-z_{1i})(n_{fi}+3)}\left[\left(z_{1i+1}-z_{1n_1}\right)^{n_{fi}+3}-\left(z_{1i}-z_{1n_1}\right)^{n_{fi}+3}\right]+ \\
& +\frac{z_{1n_1}(S_{Li}-S_{Ui})}{(z_{1i+1}-z_{1i})(n_{fi}+2)}\left[\left(z_{1i+1}-z_{1n_1}\right)^{n_{fi}+2}-\left(z_{1i}-z_{1n_1}\right)^{n_{fi}+2}\right]\Bigg\}\Bigg\}- \\
-2\sum_{i=1}^{i=n}\Bigg\{ & \frac{\kappa^{n_{fi}+1}S_{Ai}n_{fi}}{5(n_{fi}+1)(n_{fi}+2)}\left[\left(z_{3i}-z_{3n_3}\right)^{n_{fi}+2}-\left(z_{3i+1}-z_{3n_3}\right)^{n_{fi}+2}\right]+ \\
& +\frac{\kappa^{n_{fi}+1}S_{Ui}}{(n_{fi}+1)(n_{fi}+2)}\left[\left(z_{3i}-z_{3n_3}\right)^{n_{fi}+2}-\left(z_{3i+1}-z_{3n_3}\right)^{n_{fi}+2}\right]+\frac{\kappa^{n_{fi}+1}(S_{Li}-S_{Ui})}{n_{fi}+1}\Bigg\{ \frac{1}{2(n_{fi}+2)}\left[\left(z_{3i}-z_{3n_3}\right)^{n_{fi}+2}-\left(z_{3i+1}-z_{3n_3}\right)^{n_{fi}+2}\right]+ \\
& +\frac{1}{(z_{3i+1}-z_{3i})(n_{fi}+3)}\left[\left(z_{3i}-z_{3n_3}\right)^{n_{fi}+3}-\left(z_{3i+1}-z_{3n_3}\right)^{n_{fi}+3}\right]+\frac{z_{3n_3}}{(z_{3i+1}-z_{3i})(n_{fi}+2)}\left[\left(z_{3i}-z_{3n_3}\right)^{n_{fi}+2}-\left(z_{3i+1}-z_{3n_3}\right)^{n_{fi}+2}\right]\Bigg\}+ \\
& +\kappa^{n_{fi}+1}\Bigg\{ \frac{S_{Ui}}{n_{fi}+2}\left[\left(z_{3i+1}-z_{3n_3}\right)^{n_{fi}+2}-\left(z_{3i}-z_{3n_3}\right)^{n_{fi}+2}\right]+\frac{S_{Li}-S_{Ui}}{2(n_{fi}+2)}\left[\left(z_{3i+1}-z_{3n_3}\right)^{n_{fi}+2}-\left(z_{3i}-z_{3n_3}\right)^{n_{fi}+2}\right]+ \\
& +\frac{S_{Li}-S_{Ui}}{(z_{3i+1}-z_{3i})(n_{fi}+3)}\left[\left(z_{3i+1}-z_{3n_3}\right)^{n_{fi}+3}-\left(z_{3i}-z_{3n_3}\right)^{n_{fi}+3}\right]+ \\
& +\frac{z_{3n_3}(S_{Li}-S_{Ui})}{(z_{3i+1}-z_{3i})(n_{fi}+2)}\left[\left(z_{3i+1}-z_{3n_3}\right)^{n_{fi}+2}-\left(z_{3i}-z_{3n_3}\right)^{n_{fi}+2}\right]\Bigg\}\Bigg\}
\end{aligned}
\tag{21}
$$

It should be noted that at $n_{fi}=1$, $S_{Ui}=S_{Li}=E$, $S_{Ai}=0$, $h_1=h_2=h$ and $n_L=n=1$, Eq. (21) transforms in

$$G=\frac{21F^2l^2}{2Eb^2h^3} \tag{22}$$

which is exact match of the formula for strain energy release rate in linear-elastic homogeneous four-point bending beam when the crack is located in the beam mid-plane [24].

In order to verify Eq. (21), an additional analysis of the delamination fracture is performed by applying the *J*-integral approach [25]. The *J*-integral is solved by using integration contour, Γ, which is shown with dotted line in Fig. 1. It is obvious that the *J*-integral value is zero in the segment of the integration contour which coincides with the cross-section of the upper crack arm. Besides, the *J*-integral value is zero in the segments of the integration contour which coincide with upper and lower beam surfaces. Thus, the *J*-integral solution is written as:

$$J=2(J_{\Gamma_1}+J_{\Gamma_2}) \tag{23}$$

where J_{Γ_1} and J_{Γ_2} are the *J*-integral values in segments Γ_1 and Γ_2, respectively (the expression in brackets in Eq. (23) is doubled since there are two symmetric cracks (Fig. 1)).

First, the integration is carried-out in segment Γ_1 (this segment coincides with cross-section of the lower crack arm (Fig.1)). The *J*-integral in segment, Γ_1, is written as:

$$J_{\Gamma_1}=\sum_{i=1}^{n_L}\int_{z_{1i}}^{z_{1i+1}}\left[u_{0L_i}\cos\alpha-\left(p_{xi}\frac{\partial u}{\partial x}+p_{yi}\frac{\partial v}{\partial x}\right)\right]ds \tag{24}$$

where u_{0L_i} is the strain energy density in the *i*-th layer of the lower crack arm, α is the angle between the outwards normal vector to the contour of integration and the crack direction, p_{xi} and p_{yi} are the components of stress vector in the *i*-th layer of the lower crack arm, *u* and *v* are the components of displacement vector with respect to the crack tip coordinate system *xy* (*x* is directed along the crack), *ds* is a differential element along the contour.

The components of J_{Γ_1} are found as:

$$p_{xi}=-\sigma_i=-S_i\varepsilon^{n_{fi}}\quad,\quad p_{yi}=0 \tag{25}$$

$$ds=dz_1\ ,\ \cos\alpha=-1 \tag{26}$$

$$\frac{\partial u}{\partial x}=\varepsilon=\left(z_1-z_{1n_1}\right)\kappa_1 \tag{27}$$

where z_1 varies in the interval $[-h_1/2,\ h_1/2]$.

The strain energy density is equal to the area, *OPQ*, enclosed by the stress-strain curve (Fig.3)

$$u_{0L_i}=\int_0^{\varepsilon}\sigma_i d\varepsilon \tag{28}$$

By substituting of Eq. (1) in Eq. (28), one obtains

$$u_{0L_i}=\frac{S_i\varepsilon^{n_{fi}+1}}{n_{f_i}+1} \tag{29}$$

By substituting of Eqs. (2), (13), (25), (26), (27) and (29) in Eq. (24), one derives

$$J_{\Gamma_1}=\sum_{i=1}^{i=n_L}\left\{\frac{16\kappa_L^{n_{fi}+1}S_{Ai}n_{fi}y_1^4}{b^4\left(n_{fi}+1\right)\left(n_{fi}+2\right)}\left[\left(z_{1i}-z_{1n_1}\right)^{n_{fi}+2}-\left(z_{1i+1}-z_{1n_1}\right)^{n_{fi}+2}\right]+\right.$$
$$+\frac{\kappa_L^{n_{fi}+1}S_{Ui}y_1}{\left(n_{fi}+1\right)\left(n_{fi}+2\right)}\left[\left(z_{1i}-z_{1n_1}\right)^{n_{fi}+2}-\left(z_{1i+1}-z_{1n_1}\right)^{n_{fi}+2}\right]+$$
$$+\frac{\kappa_L^{n_{fi}+1}\left(S_{Li}-S_{Ui}\right)y_1}{n_{fi}+1}\left\{\frac{1}{2\left(n_{fi}+2\right)}\left[\left(z_{1i}-z_{1n_1}\right)^{n_{fi}+2}-\left(z_{1i+1}-z_{1n_1}\right)^{n_{fi}+2}\right]+\right.$$
$$+\frac{1}{\left(z_{1i+1}-z_{1i}\right)\left(n_{fi}+3\right)}\left[\left(z_{1i}-z_{1n_1}\right)^{n_{fi}+3}-\left(z_{1i+1}-z_{1n_1}\right)^{n_{fi}+3}\right]+$$
$$\left.+\frac{z_{1n_1}}{\left(z_{1i+1}-z_{1i}\right)\left(n_{fi}+2\right)}\left[\left(z_{1i}-z_{1n_1}\right)^{n_{fi}+2}-\left(z_{1i+1}-z_{1n_1}\right)^{n_{fi}+2}\right]\right\}+\kappa_L^{n_{fi}+1}y_1\left\{\frac{S_{Ui}}{n_{fi}+2}\left[\left(z_{1i+1}-z_{1n_1}\right)^{n_{fi}+2}-\left(z_{1i}-z_{1n_1}\right)^{n_{fi}+2}\right]+\right.$$
$$+\frac{S_{Li}-S_{Ui}}{2\left(n_{fi}+2\right)}\left[\left(z_{1i+1}-z_{1n_1}\right)^{n_{fi}+2}-\left(z_{1i}-z_{1n_1}\right)^{n_{fi}+2}\right]+\frac{S_{Li}-S_{Ui}}{\left(z_{1i+1}-z_{1i}\right)\left(n_{fi}+3\right)}\left[\left(z_{1i+1}-z_{1n_1}\right)^{n_{fi}+3}-\left(z_{1i}-z_{1n_1}\right)^{n_{fi}+3}\right]+$$
$$\left.\left.+\frac{z_{1n_1}\left(S_{Li}-S_{Ui}\right)}{\left(z_{1i+1}-z_{1i}\right)\left(n_{fi}+2\right)}\left[\left(z_{1i+1}-z_{1n_1}\right)^{n_{fi}+2}-\left(z_{1i}-z_{1n_1}\right)^{n_{fi}+2}\right]\right\}\right\} \tag{30}$$

Eq. (30) can also be used to obtain the *J*-integral solution in segment, Γ_2, of the integration contour (Fig. 1). For this purpose, z_{1i}, z_{1i+1}, n_L, κ_L and z_{1n_1} should be replaced with z_{3i}, z_{3i+1}, n, κ and z_{3n_3}, respectively. Besides, the sign of Eq. (30) must be set to "minus" because the integration contour is directed upwards in segment, Γ_2.

Finally, J_{Γ_1} and J_{Γ_2} are substituted in Eq. (23)

$$J=2\sum_{i=1}^{i=n_L}\left\{\frac{16\kappa_L^{n_{fi}+1}S_{Ai}n_{fi}y_1^4}{b^4\left(n_{fi}+1\right)\left(n_{fi}+2\right)}\left[\left(z_{1i}-z_{1n_1}\right)^{n_{fi}+2}-\left(z_{1i+1}-z_{1n_1}\right)^{n_{fi}+2}\right]+\right.$$
$$+\frac{\kappa_L^{n_{fi}+1}S_{Ui}y_1}{\left(n_{fi}+1\right)\left(n_{fi}+2\right)}\left[\left(z_{1i}-z_{1n_1}\right)^{n_{fi}+2}-\left(z_{1i+1}-z_{1n_1}\right)^{n_{fi}+2}\right]+$$
$$+\frac{\kappa_L^{n_{fi}+1}\left(S_{Li}-S_{Ui}\right)y_1}{n_{fi}+1}\left\{\frac{1}{2\left(n_{fi}+2\right)}\left[\left(z_{1i}-z_{1n_1}\right)^{n_{fi}+2}-\left(z_{1i+1}-z_{1n_1}\right)^{n_{fi}+2}\right]+\right.$$
$$+\frac{1}{\left(z_{1i+1}-z_{1i}\right)\left(n_{fi}+3\right)}\left[\left(z_{1i}-z_{1n_1}\right)^{n_{fi}+3}-\left(z_{1i+1}-z_{1n_1}\right)^{n_{fi}+3}\right]+$$
$$\left.+\frac{z_{1n_1}}{\left(z_{1i+1}-z_{1i}\right)\left(n_{fi}+2\right)}\left[\left(z_{1i}-z_{1n_1}\right)^{n_{fi}+2}-\left(z_{1i+1}-z_{1n_1}\right)^{n_{fi}+2}\right]\right\}+$$
$$+\kappa_L^{n_{fi}+1}y_1\left\{\frac{S_{Ui}}{n_{fi}+2}\left[\left(z_{1i+1}-z_{1n_1}\right)^{n_{fi}+2}-\left(z_{1i}-z_{1n_1}\right)^{n_{fi}+2}\right]+\frac{S_{Li}-S_{Ui}}{2\left(n_{fi}+2\right)}\left[\left(z_{1i+1}-z_{1n_1}\right)^{n_{fi}+2}-\left(z_{1i}-z_{1n_1}\right)^{n_{fi}+2}\right]+\right.$$
$$+\frac{S_{Li}-S_{Ui}}{\left(z_{1i+1}-z_{1i}\right)\left(n_{fi}+3\right)}\left[\left(z_{1i+1}-z_{1n_1}\right)^{n_{fi}+3}-\left(z_{1i}-z_{1n_1}\right)^{n_{fi}+3}\right]+$$
$$\left.\left.+\frac{z_{1n_1}\left(S_{Li}-S_{Ui}\right)}{\left(z_{1i+1}-z_{1i}\right)\left(n_{fi}+2\right)}\left[\left(z_{1i+1}-z_{1n_1}\right)^{n_{fi}+2}-\left(z_{1i}-z_{1n_1}\right)^{n_{fi}+2}\right]\right\}\right\}- \tag{31}$$

$$
\begin{aligned}
-2\sum_{i=1}^{i=n}\Bigg\{ & \frac{16\kappa^{n_{fi}+1}S_{Ai}n_{fi}y_1^4}{b^4(n_{fi}+1)(n_{fi}+2)}\Big[\left(z_{3i}-z_{3n_3}\right)^{n_{fi}+2}-\left(z_{3i+1}-z_{3n_3}\right)^{n_{fi}+2}\Big]+ \\
& +\frac{\kappa^{n_{fi}+1}S_{Ui}y_1}{(n_{fi}+1)(n_{fi}+2)}\Big[\left(z_{3i}-z_{3n_3}\right)^{n_{fi}+2}-\left(z_{3i+1}-z_{3n_3}\right)^{n_{fi}+2}\Big]+ \\
& +\frac{\kappa^{n_{fi}+1}(S_{Li}-S_{Ui})y_1}{n_{fi}+1}\Bigg\{\frac{1}{2(n_{fi}+2)}\Big[\left(z_{3i}-z_{3n_3}\right)^{n_{fi}+2}-\left(z_{3i+1}-z_{3n_3}\right)^{n_{fi}+2}\Big]+ \\
& +\frac{1}{(z_{3i+1}-z_{3i})(n_{fi}+3)}\Big[\left(z_{3i}-z_{3n_3}\right)^{n_{fi}+3}-\left(z_{3i+1}-z_{3n_3}\right)^{n_{fi}+3}\Big]+\frac{z_{3n_3}}{(z_{3i+1}-z_{3i})(n_{fi}+2)}\Big[\left(z_{3i}-z_{3n_3}\right)^{n_{fi}+2}-\left(z_{3i+1}-z_{3n_3}\right)^{n_{fi}+2}\Big]\Bigg\}+ \\
& +\kappa^{n_{fi}+1}y_1\Bigg\{\frac{S_{Ui}}{n_{fi}+2}\Big[\left(z_{3i+1}-z_{3n_3}\right)^{n_{fi}+2}-\left(z_{3i}-z_{3n_3}\right)^{n_{fi}+2}\Big]+\frac{S_{Li}-S_{Ui}}{2(n_{fi}+2)}\Big[\left(z_{3i+1}-z_{3n_3}\right)^{n_{fi}+2}-\left(z_{3i}-z_{3n_3}\right)^{n_{fi}+2}\Big]+ \\
& +\frac{S_{Li}-S_{Ui}}{(z_{3i+1}-z_{3i})(n_{fi}+3)}\Big[\left(z_{3i+1}-z_{3n_3}\right)^{n_{fi}+3}-\left(z_{3i}-z_{3n_3}\right)^{n_{fi}+3}\Big]+ \\
& +\frac{z_{3n_3}(S_{Li}-S_{Ui})}{(z_{3i+1}-z_{3i})(n_{fi}+2)}\Big[\left(z_{3i+1}-z_{3n_3}\right)^{n_{fi}+2}-\left(z_{3i}-z_{3n_3}\right)^{n_{fi}+2}\Big]\Bigg\}\Bigg\}
\end{aligned}
\tag{31}
$$

It should be noted that Eq. (31) describes the distribution of the *J*-integral value along the crack front. The average value of the *J*-integral along the crack front is written as:

$$
J_{av}=\frac{1}{b}\int_{-\frac{b}{2}}^{\frac{b}{2}}J\,dy_1 \tag{32}
$$

The solution of the *J*-integral derived by substituting of Eq. (31) in Eq. (32) is exact match of Eq. (21). This fact verifies the delamination fracture analysis developed in the present paper.

The effects of crack location along the beam cross-section height, material gradient and the non-linear behaviour of material on the delamination fracture in the functionally graded multilayered four-point bending beam configuration are elucidated. For this purpose, parametric analyses of the delamination behaviour are performed. The strain energy release rate is calculated by Eq. (21). In order to assess the influence of crack location, two three-layered beam configurations are considered (Fig. 4). The delamination crack is located between layers 1 and 2 in the beam configuration shown in Fig. 4(a). In the beam configuration in Fig. 4(b) the delamination is between layers 2 and 3. The thickness of each layer is t_l. It is assumed that b=0.02m, $t_l=0.005\,m$, h=0.0075m, $n_{f1}=n_{f2}=n_{f3}=0.65$, $F=40\,N$ and l=0.1m. The strain energy release rate calculated is presented in non-dimensional form by using the formula, $G_N=G/(S_{U1}b)$.

The material gradient along the thickness of layer 3 is characterized by S_{L1}/S_{U1} ratio. It should be noted that S_{U1} is kept constant in the calculations. Therefore, S_{L1} is varied in order to generate various S_{L1}/S_{U1} ratios. The strain energy release rate in non-dimensional form is plotted against S_{L1}/S_{U1} ratio for $S_{A1}/S_{U1}=1.5$, $S_{U2}/S_{U1}=1.2$, $S_{L2}/S_{U2}=0.5$, $S_{A2}/S_{U2}=0.5$, $S_{U3}/S_{U1}=0.8$, $S_{L3}/S_{U3}=0.6$ and $S_{A3}/S_{U3}=1.5$ in Fig. 5. Calculations are carried-out for both beam configurations shown in Fig. 4. The curves in Fig. 5 indicate that the strain energy release rate decreases with increasing S_{L1}/S_{U1} ratio. This finding is attributed to the decrease of the beam stiffness. It can also be observed in Fig. 5 that the strain energy release rate is higher when the delamination crack is located between layers 2 and 3. Therefore, it can be concluded that the strain energy release rate increases with decreasing of the lower crack arm thickness.

The influence of material gradient along the beam width in layer 2 is also analyzed (this gradient is characterized by S_{A2}/S_{U2} ratio). For this purpose, the strain energy release rate in non-dimensional form is presented as a

function of S_{A2}/S_{U2} ratio for two S_{L2}/S_{U2} ratios at $S_{L1}/S_{U1}=0.5$, $S_{A1}/S_{U1}=1.4$, $S_{U2}/S_{U1}=1.3$, $S_{U3}/S_{U1}=0.6$, $S_{L3}/S_{U3}=0.8$ and $S_{A3}/S_{U3}=1.3$ in Fig. 6. The beam configuration shown in Fig. 4(b) is analyzed. One can observe that the strain energy release rate decreases with increasing of S_{A2}/S_{U2} and S_{L2}/S_{U2} ratios (Fig. 6).

The influence of S_{U3}/S_{U1} ratio on the strain energy release rate is investigated too. For this purpose, the strain energy release rate in non-dimensional form is plotted against S_{U3}/S_{U1} ratio at $S_{A1}/S_{U1}=1.1$, $S_{L1}/S_{U1}=0.4$, $S_{U2}/S_{U1}=1.1$, $S_{L2}/S_{U2}=0.6$, $S_{A2}/S_{U2}=0.6$, $S_{L3}/S_{U3}=0.4$ and $S_{A3}/S_{U3}=0.9$ in Fig. 7. The beam configuration shown in Fig. 4(b) is considered. The curves in Fig. 7 indicate that the strain energy release rate decreases with increasing of S_{U3}/S_{U1} ratio. In order to elucidate the effect of non-linear behaviour of the material on the delamination fracture, the strain energy release rate in non-dimensional form obtained assuming linear-elastic material behaviour of functionally graded multilayered beam is presented as a function of S_{U3}/S_{U1} ratio in Fig. 7 for comparison (the linear-elastic solution is derived by substituting of $n_{fi}=1$ in Eq. (21)). It can be observed that the non-linear behaviour of the material leads to increase of the strain energy release rate (Fig. 7).

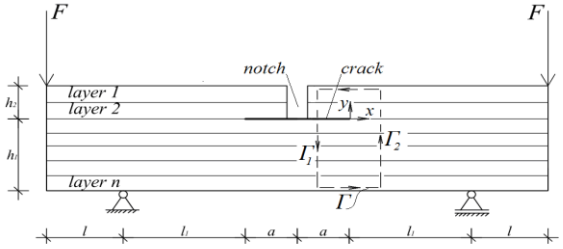

Fig.1
Geometry and loading of a multilayered functionally graded four-point bending beam.

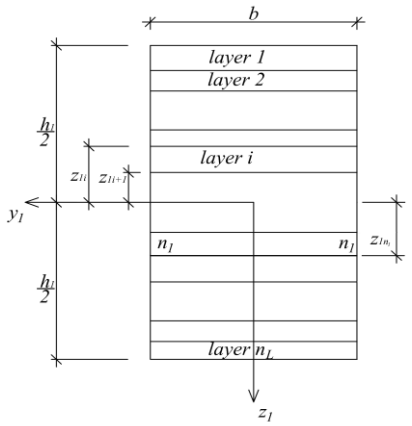

Fig.2
Lower crack arm cross-section (n_1-n_1 is the neutral axis).

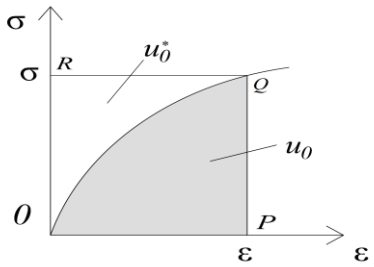

Fig.3
Non-linear stress-strain curve (u_0 and u_0^* are the strain energy density and complementary strain energy density, respectively).

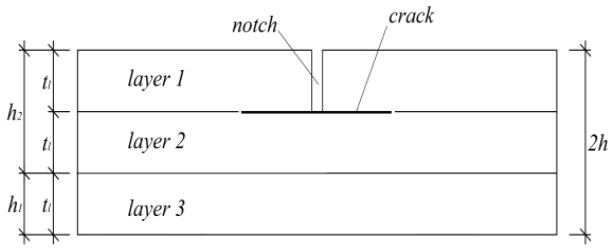

(a)

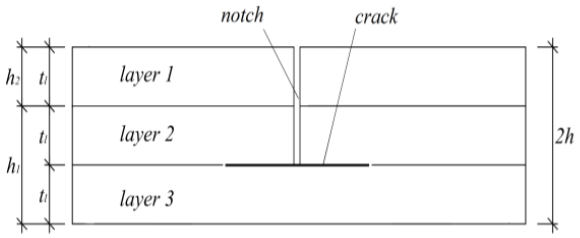

(b)

Fig.4
Two three-layered functionally graded beam configurations.

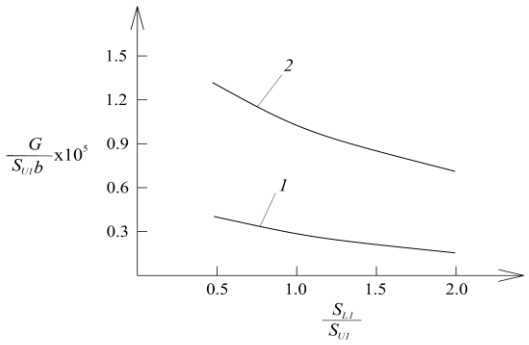

Fig.5
The strain energy release rate in non-dimensional form plotted against S_{L1}/S_{U1} ratio (curve 1 – for the beam shown in Fig. 4(a), curve 2 - for the beam in Fig. 4(b).

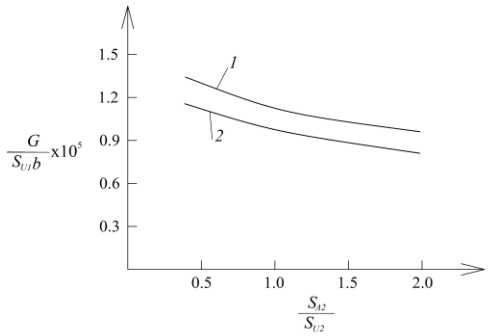

Fig.6
The strain energy release rate in non-dimensional form plotted against S_{A2}/S_{U2} ratio (curve 1 – for $S_{L2}/S_{U2}=0.5$, curve 2 – for $S_{L2}/S_{U2}=1.5$).

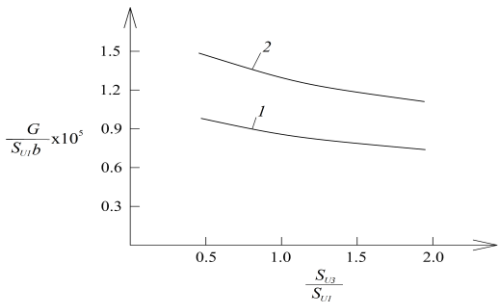

Fig.7
The strain energy release rate in non-dimensional form presented as a function of S_{U3}/S_{U1} ratio (curve 1 – at linear-elastic behaviour of material, curve 2 – at non-linear behaviour of material).

3 CONCLUSIONS

The delamination fracture in functionally graded multilayered four-point bending beam configuration is analyzed in terms of the strain energy release rate with taking into account the non-linear behaviour of material. The beam may have an arbitrary number of layers. Each layer has different thickness and material properties. Besides, the material is two-dimensional functionally graded in the cross-section of each layer. A delamination crack is located arbitrary

between layers. The beam mechanical behaviour is described by a power-law stress-strain relation. The analytical solution to the strain energy release rate derived is verified by analyzing the delamination fracture with the help of the *J*-integral. The solution is used to elucidate the effects of crack location, material gradients and non-linear behaviour of material on the delamination fracture. The analysis reveals that the strain energy release rate increases with decreasing of the lower crack arm thickness. It is found also that the non-linear behaviour of material leads to increase of the strain energy release rate. This finding indicates that the non-linear behaviour has to be taken into account for an efficient and safe design of structural members and components made of two-dimensional functionally graded multilayered materials. The parametric investigation reveals also that the strain energy release rate can be regulated effectively by employing appropriate material gradients in the design stage of functionally graded multilayered structures and components.

REFERENCES

[1] Koizumi M., 1993, The concept of FGM ceramic trans, *Functionally Gradient Materials* **34**(2): 3-10.

[2] Suresh S., Mortensen A., 1998, *Fundamentals of Functionally Graded Materials*, IOM Communications Ltd, London.

[3] Levashov E.A., Larikin D.V., Shtansky D.V., Rogachev A.S., Grigorian H.E., Moore J.J., 2002, Self-propagating high-temperature synthesis of functionally graded PVD targets with a ceramic working layer of TiB-TiN or TiSi-Tin, *Journal of Materials Synthesis and Processing* **10**(2): 319.

[4] Tokova L., Yasinskyy A., Ma C. C., 2016, Effect of the layer inhomogeneity on the distribution of stresses and displacements in an elastic multilayer cylinder, *Acta Mechanica* **228**: 2865-2877.

[5] Tokovyy Y., Ma C. C., 2013, Three-dimensional temperature and thermal stress analysis of an inhomogeneous layer, *Journal of Thermal Stresses* **36**: 790- 808.

[6] Tokovyy Y., Ma C. C., 2016, Axisymmetric stresses in an elastic radially inhomogeneous cylinder under length-varying loadings, *ASME Journal of Applied Mechanics* **83**: 111007-111013.

[7] Uslu Uysal M., Kremzer M., 2015, Buckling behaviour of short cylindrical functionally gradient polymeric materials, *Acta Physica Polonica A* **127**: 1355-1357.

[8] Uslu Uysal M., 2016, Buckling behaviours of functionally graded polymeric thin-walled hemispherical shells, *Steel and Composite Structures, An International Journal* **21**: 849-862.

[9] Szekrenyes A., 2010, Fracture analysis in the modified split-cantilever beam using the classical theories of strength of materials, *Journal of Physics: Conference Series* 240(4): 012030.

[10] Szekrenyes A., 2016, Semi-layerwise analysis of laminated plates with nonsingular delamination - the theorem of autocontinuity, *Applied Mathematical Modelling* **40**(2): 1344-1371.

[11] Paulino G.C., 2002, Fracture in functionally graded materials, *Engineering Fracture Mechanics* **69**(2): 1519-1530.

[12] Tilbrook M.T., Moon R.J., Hoffman M., 2005, Crack propagation in graded composites, *Composite Science and Technology* **65**(2): 201-220.

[13] Carpinteri A., Pugno N., 2006, Cracks in re-entrant corners in functionally graded materials, *Engineering Fracture Mechanics* **73**(4): 1279-1291.

[14] Upadhyay A.K., Simha K.R.Y., 2007, Equivalent homogeneous variable depth beams for cracked FGM beams; compliance approach, *International Journal of Fracture* **144**(4): 209-213.

[15] Zhang H., Li X.F., Tang G.J., Shen Z.B., 2013, Stress intensity factors of double cantilever nanobeams via gradient elasticity theory, *Engineering Fracture Mechanics* **105**(4): 58-64.

[16] Uslu Uysal M., Güven U., 2016, A bonded plate having orthotropic inclusion in adhesive layer under in-plane shear loading, *The Journal of Adhesion* **92**(2): 214-235.

[17] Dahan I., Admon U., Sarei J., Yahav B., Amar M., Frage N., Dariel M. P., 1999, Functionally graded Ti-TiC multilayers: the effect of a graded profile on adhesion to substrate, *Materials Science Forum* **308-311**(3): 923-929.

[18] Bora Y., Suphi Y., Suat K., 2008, Material coatings under thermal loading, *Journal of Applied Mechanics* **75**(4): 051106.

[19] Sung Ryul Ch., Hutchinson J.W., Evans A.G., 1999, Delamination of multilayer thermal barrier coatings, *Mechanics of Materials* **31**(3): 431-447.

[20] Szekrenyes A., 2016, Nonsingular crack modelling in orthotropic plates by four equivalent single layers, *European Journal of Mechanics – A/Solids* **55**: 73-99.

[21] Petrov V.V., 2014, *Non-Linear Incremental Structural Mechanics*, Infra-Injeneria.

[22] Lubliner J., 2006, *Plasticity Theory*, University of California, Berkeley.

[23] Dowling N., 2007, *Mechanical Behavior of Materials*, Pearson.

[24] Hutchinson W., Suo Z., 1992, Mixed mode cracking in layered materials, *Advances in Applied Mechanics* **64**(3): 804-810.

[25] Broek D., 1986, *Elementary Engineering Fracture Mechanics*, Springer.